Determination of the microtexture of reinforced thermoplastics by image analysis

Luc Avérous, Jean-christophe Quantin, A Crespy

DETERMINATION OF THE MICROTEXTURE OF REINFORCED THERMOPLASTICS BY IMAGE ANALYSIS

Luc Avérous, Jean-Christophe Quantin* & Alain Crespy

Ecole des Mines d'Alès, Laboratoire Matrices-Matériaux Minéraux et Organiques, 6 avenue de Clavières, 30319 Alès, France

Abstract

The mechanical properties of reinforced thermoplastics depend on such characteristics of the filler as granulometry, orientation and dispersion. These different microtextural parameters were determined by using a single tool: image analysis, which was coupled with optical and electron microscopies. The different materials tested were based on short-glass-fibre-reinforced polypropylene obtained by extrusion and injection steps. For the different samples analysed, the processing conditions and the filler concentration were constant, and variability was due to the different average lengths of the filler incorporated in the matrix. The different filler parameters were determined with particular emphasis on the techniques of dispersion characterisation. The techniques developed in this study were based on image analysis. They enabled us to estimate filler-size distribution and development of the three-dimensional orientation inside the material and between different samples. The development of the filler dispersion was also made apparent. In addition, the relationships obtained between the different microtextural parameters were investigated. The general conclusion is that image analysis is very suitable for characterisation of this kind of material.

Keywords: A. short-fibre composites, B. microstructure, D. optical microscopy, D. scanning electron micro-scopy, E. injection moulding

1 INTRODUCTION

Reinforced thermoplastics are produced by incorporat-ing reinforcing fillers into the polymeric matrix in order to improve material properties such as mechanical strength. These materials are being used increasingly in applications where high performance is essential. The properties of such materials depend largely on the dis-tribution of the filler in the matrix. It is therefore important to be able to analyse precisely the different characteristics of the filler inside the thermoplastic.

The principal aim of this study was to measure the different filler characteristics that may affect the properties of reinforced thermoplastics. These different and influential parameters are defined as microtextural parameters.[1]

1.1 Microtexture—a definition

Generally, a model takes into account only the main elements of the systems that it is expected to describe. The analysis of models predicting the mechanical properties of composite materials (Young's modulus, toughness, etc.) could provide a data base for the principal characteristics of reinforcements. To select the main parameters of the filler, different mechanical models were examined.[1] For example, most fibre composite models require the orientation and length of the fibre, such as the standard Krenchel[2] and Cox[3] rule of mixtures used for evaluation of the Young's modulus of the composite as in eqn (1):

$$E_{\text{composite}} = \eta_l \times \eta_\theta \times E_\text{f} \times (1 - v_\text{f})E_\text{m} \qquad (1)$$

The factors η_l and η_θ are functions respectively of the length and orientation of the fibre. E_f and E_m are the fibre and matrix Young's moduli, v_f is the fibre volume fraction.

In addition to the filler's geometrical parameters and orientation factors, another type of parameter affects the material's mechanical properties:[4] the dispersion of the filler inside the matrix. To establish a definition, we isolated each parameter of the filler, thus determining the material's microtexture. We can define the microtextural characteristics as follows:

- the principal intrinsic parameters of the filler such as the size (granulometry) and shape (granulomorphy); and
- the spatial organisation parameters of the filler in the matrix, described by the orientation and the dispersion.

To determine these different microtextural parameters, we used a single powerful tool: image analysis

*To whom correspondence should be addressed.

coupled with microscopy which was appropriate to the determinations required. To date, image analysis techniques have been little used in the field of reinforced thermoplastics and composites.[1,4,5,7–16] Nowadays, these tools show considerable potential because of the fast acceleration in computer processors, the development of powerful algorithms and the improving accessibility of these techniques.

1.2 Image analysis[5,6]

Images are complex sets of various interconnected data. For a long time, human beings were not able to quantify morphological information, except by extending their own vision system by means of geometrical measurement devices. Now, thanks to improvements in the coupling of microelectronics and computer science, automatic image treatment and analysis systems can be designed. Image analysis is based on mathematical concepts that provide a quantitative approach to the image. The techniques and methods employed depend on the type of information to be extracted and analysed, whichever image is studied. In general, two main types of application can be distinguished:

- shape recognition, which identifies shapes according to different models; and
- quantitative image analysis, which consists of analysis and quantification of morphological structure.

Like human vision, quantitative image analysis consists of three main stages.

- Image acquisition: the different images are obtained through a charge-coupled device (CCD) camera and then digitised with a special frame grabber. The typical format of the image is 512×512 pixels with 256 shades of grey. Each pixel is coded as a byte.
- Image treatment (filtering–thresholding): a first stage of image correction is required to eliminate deformations in the image. Then, the image is filtered to increase the contrast and to correct most of the heterogeneities in brightness on the image, which might be caused by the acquisition conditions. To select the information due to the particles, the image is then thresholded. Each pixel is coded as a bit. After this phase, the image is transformed in order to extract the information needed.
- Quantitative analysis: this stage completes the image analysis procedure. It involves all the measurements required.

Our strategy in this study was to prepare different reinforced thermoplastics, keeping constant both the filler ratio and the processing conditions. Only the mean length of the filler was varied from one sample to another. We analyse the influence of this variation on the other microtextural parameters such as orientation and dispersion, in order to investigate the relationships between them. The results of the image analysis not only reveal the characteristics of the material studied but can also be used to correlate the different mechanical characteristics.

2 MATERIALS

Short-glass-fibre-reinforced polypropylene was used. Because of the fibres' shape, their orientation distribution could be determined. A polypropylene-based matrix was used because it is a very common thermoplastic. In addition, it gives good electronic and optical contrast with the glass fibres for the image-acquisition stage.

2.1 Generation of short glass fibres

Different length distributions of glass fibres were obtained by using different generation processes. A first batch was obtained from 4·5 mm cut thread (CFg). Two other batches of shorter fibres were obtained by a fragmentation process. After pneumatic fragmentation and selection (Alpine ATP50 Rotoflex; Ausburg, Germany), the powder (ground glass) was eliminated leaving only fibres, coded SFg1. A second pneumatic selection was carried out on SFg1. The fraction containing the longest fibres was eliminated and the resulting fibres were called SFg2. Three different populations of glass fibres were obtained with different average lengths (CFg, SFg1 and SFg2). They have a diameter of 14 μm.

2.2 Preparation of reinforced polypropylene specimens

The different reinforced polypropylenes were prepared with Appryl 3030 MN1 resin (Atochem, France). The weight-average molecular weight of this isotactic polypropylene homopolymer was 325 000 Daltons. The fibre content for all the samples produced was close to 30 wt% (see Table 2). Processing conditions were identical for all the specimens. A two-stage process was used to produce injected dumb-bells. Fibre/polypropylene pellets were prepared with a co-rotating twin-screw extruder (Clextral BC 45; Firminy, France). An injection moulding machine (Billion; Bellignat, France) with a clamping force of 950 kN was used to mould standard dumb-bells. These have a calibrated part 10 mm wide and 4 mm thick (according to French standard NFT 51-034 1981). The different samples were taken from the central part of the dumb-bells.

3 MICROTEXTURAL DETERMINATIONS

Three kinds of determination were carried out on dumb-bell specimens to get the different microtextural parameters: a granulometric determination (measurement of the fibre length distribution) and two determinations

of both the three-dimensional (3D) orientation and the dispersion of the fibres in the matrix.

3.1 Granulometric determinations

To assess fibre granulometry it is important to calculate not only the mean length but also the size distribution. To do this, we developed an automatic technique by coupling optical microscopy and image analysis. The suggested granulometric techniques and the main results are described in a recent paper.[10]

To separate the fibres from the matrix, the material was pyrolysed in a muffle furnace for 2 h at 500°C. The fibres were spread between two glass microscope slides. Images were acquired with a polarising microscope in transmission mode coupled with a CCD camera (see Fig. 1). Then, image treatment and quantitative analysis were performed.

It is important to notice that the size parameter was chosen according to the geometry of the filler. In the case of a fibre, the geometry is close to a cylinder. Thus the selected size factor is the exodiameter, which is estimated from the maximum Feret's diameter. The Feret's diameter is, in the plane, the length a particle projects in a given direction.[5] For each analysis, a population of at least 800 fibres was treated and analysed. Usually, granulometry offers two kinds of representation. In the first, all the particles analysed are equally weighted. The distribution can be expressed by the arithmetic average length, L_n, according to eqn (2). In the second, each particle is weighted according to its length. The distribution can be expressed by the average length in weight, L_w, as in eqn (3).

$$L_n = \frac{\sum_i d_i \times n_i}{\sum_i n_i} \tag{2}$$

$$L_w = \frac{\sum_i d_i^2 \times n_i}{\sum_i d_i \times n_i} \tag{3}$$

where n_i is the number of fibres and d_i is the maximum Feret's diameter.

3.2 Granulomorphic determinations[17]

For granulomorphic determinations, the shape parameter of each particle was obtained by determining, for instance, the ratio between the exodiameter and the mesodiameter, which corresponds to the minimum Feret's diameter. In the case of a fibre, the minimum Feret's diameter is its actual diameter. In our case this was not an additional determination because only fibres of the same diameter had been treated. Thus the granulomorphy was equivalent to the granulometry.

4 THREE-DIMENSIONAL ORIENTATION DETERMINATIONS

This technique and the main results obtained are described in some recent papers.[14,15] The orientation of an anisotropic particle in the matrix can be described by two angles: the inclination and in-plane angles in a spherical coordinate system (see Fig. 2). To determine these, an original semi-automatic technique was developed by coupling scanning electron microscopy (SEM) and image analysis. To determine the orientation angles of fibres, their elliptical marks on a sectioned polished surface were used (see Fig. 3). From the SEM image, 256 grey-level images (see Fig. 4) were transferred to the image analyser. After treatment, quantitative analysis can give orientation results that can be expressed in different ways (plano-spherical representations, orientation

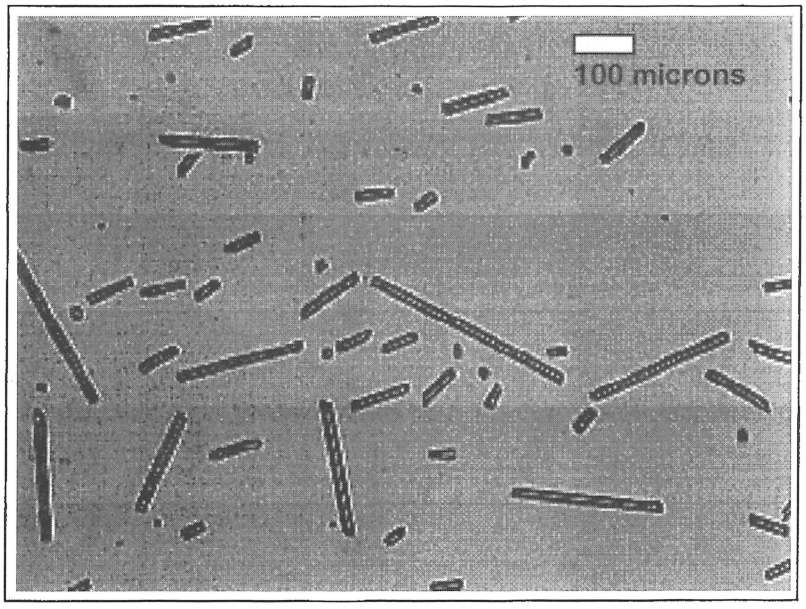

Fig. 1. Image of dispersed fibres between two glass slides.

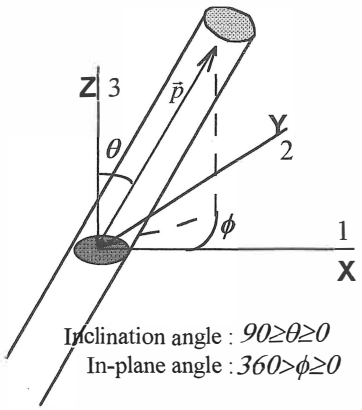

Fig. 2. Description of the orientation of a fibre.

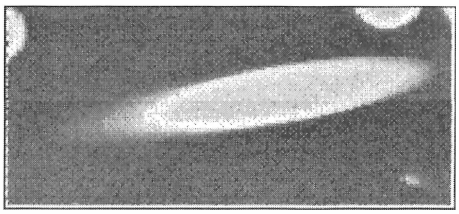

Fig. 3. Image of the elliptical mark of a fibre on a polished surface.

tensor data). The fibre is represented by a unit vector $p \rightarrow$ (see Fig. 2). The second-order tensor is given in a discrete form by eqn (4),[18,19] where n is the number of fibres studied and i,j represent the different axes (from 1 to 3).

$$a_{ij} = \frac{1}{n} \sum_{n} p_i p_j \tag{4}$$

5 DISPERSION DETERMINATIONS

Compared with the orientation, the dispersion is a less well defined notion. The dispersion corresponds to the disposition of the different fillers inside the matrix. According to the literature, the dispersion of fillers or particles in a matrix can be defined by different approaches[5,16,20,21] such as:

- the spatial position distribution of the centres of gravity of the particles (without taking into account the size and shape of the particle);
- the border-to-border distances of the particles;
- the distances to the nearest particle, or to the n closest neighbours;
- the size distribution of the interparticle gaps; and
- the local filler concentrations or the local density.

All of these approaches are involved in the definition of dispersion. The approach selected depends mainly on the final use. Determinations were performed on images taken in a two-dimensional (2D) space (see Fig. 5) consisting of polished sectioned surfaces of the sample. The section was perpendicular to the injection flow direction.

Semi-automatic techniques were developed by coupling SEM and image analysis to determine:

- the area fractions;
- the interparticle distances from centre to centre; and
- the interparticle distances from border to border.

5.1 Area fraction determinations

This approach is based on analysis of the variation of filler area fraction on the surface of the sample studied. The area fraction is defined as the ratio between the area occupied by the filler and the frame area. The associated image treatment is rather easy. After thresholding the grey-level image (Figs 5 and 6), the fraction area was calculated.

The most important limitations of this method arise from variations in the area measurements at the different stages of acquisition and image treatment.

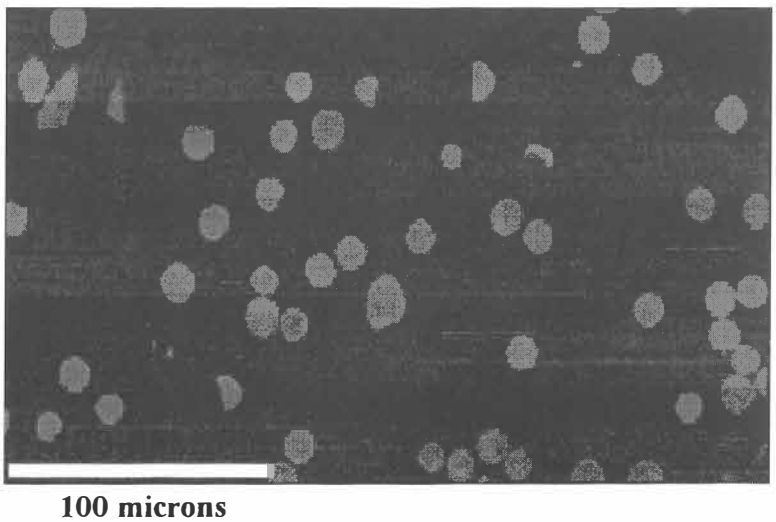

Fig. 4. SEM image of a polished section for orientation determinations.

5.2 Punctual processes (intercentre distances and stochastic models)

The purpose of this approach is to compare a punctual process consisting of the positioning of the centre of gravity of each particle in a 2D space with a stochastic punctual model, which is fully described through a few parameters. Several different punctual models have been described in the literature.[5,6,22–25] Poisson's model and its derivatives were particularly studied.

- The Poisson's model (see Fig. 7): the points are uniformly distributed in the space. Each point implantation is a fully independent process. The model is totally described by one parameter: the density of points, λ. In a two-dimensional space, the average distance, d_{1c}, to the closest point is given by eqn (5). The corresponding variance estimation, $E(s_{1c}^2)$, is given by eqn (6)

$$d_{1c} = \frac{1}{2\sqrt{\lambda}} \tag{5}$$

$$E(s_{1c}^2) = \frac{4 - \pi 1}{4\pi\lambda} \tag{6}$$

- The hard-core model (see Fig. 7): derived from the Poisson's model, it is defined by two parameters—the point density, λ, and the radius of the hard core, r_{hc}. In this model a point is taken into account only if there is no point at a distance shorter than $2r_{hc}$.

Schwartz and Exner[20] have defined two parameters, R and Q, which allow an experimental dispersion to be compared with a Poisson's process of the same density, λ. Q is the ratio between experimental d_{1c} (observed) and calculated d_{1c} [eqn (5)]. R is the ratio between the experimental variance s_{1c}^2 (observed) and the calculated variance s_{1c}^2 [eqn (6)]. For a Poisson's model $Q = 1$ and $R = 1$, and in a hard-core case $Q > 1$ and $R < 1$. This approach requires a special image treatment; on the frame each particle must be identified and reduced to one point called the centroid, which is the centre of

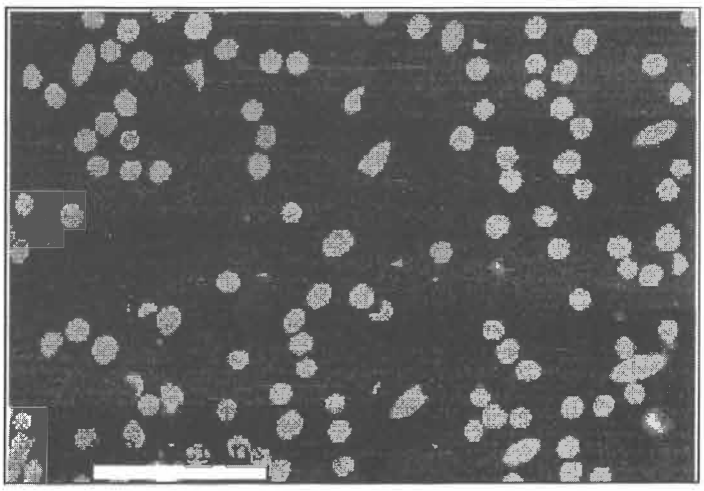

Fig. 5. SEM image of a polished section for dispersion determinations. SFg1 material.

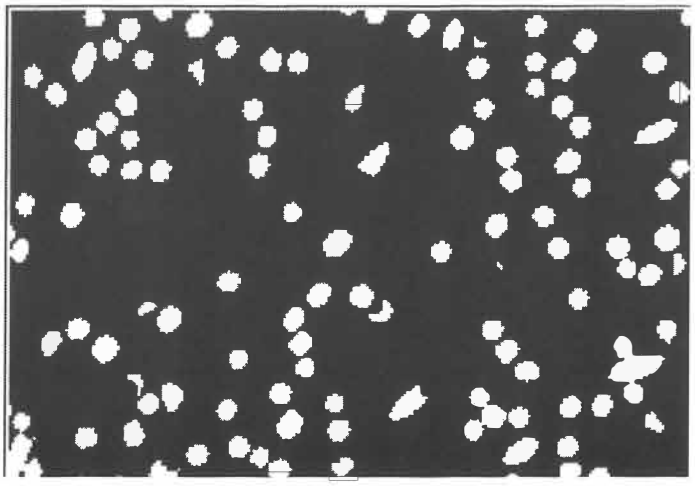

Fig. 6. Binary image corresponding to the grey-level image presented in Fig. 5.

gravity (see Fig. 8). To calculate d_{1c}, the coordinates of each point are determined to calculate the various intercentre distances, in order to select the shortest.

The limitations of this method are due to the individualisation stage and the determination of the position of the centroid of each particle.

5.3 Determination of the closest interparticle distance from border to border, d_{1b}

In contrast with the previous process, the border-to-border determination takes into account the spaces between particles in the same way mechanical models (for instance, finite element models) take into account the interparticle space where the deformations are the highest.

The method we have developed is based on a morphological approach.[6,23] The different objects on the image are treated together. The image is then considered as a mathematical set of different objects interacting with each other. The morphological mathematics uses set theory to transform the image. In our case the size of the interparticle space ought to be analysed. The inclusion

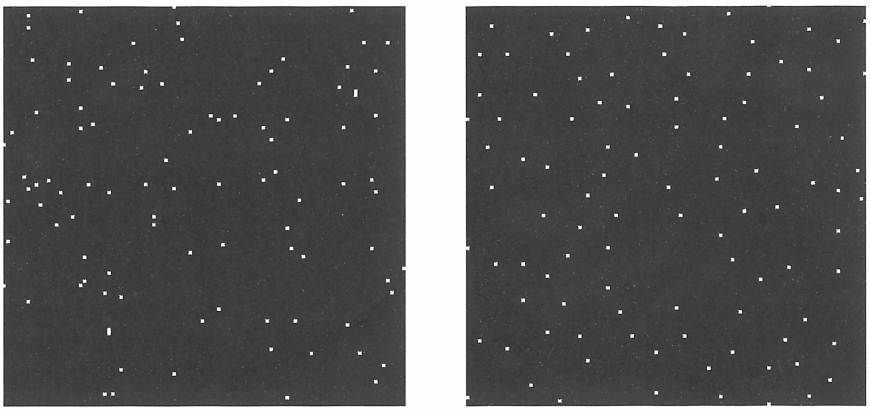

Poisson's process

Image: 100x100 pixels

Setting up of 100 points

Hard-core process

Image: 100x100 pixels

Setting up of 100 points

Exclusion radius: 6 pixels

Fig. 7. Generated images corresponding to Poisson's and hard-core processes.

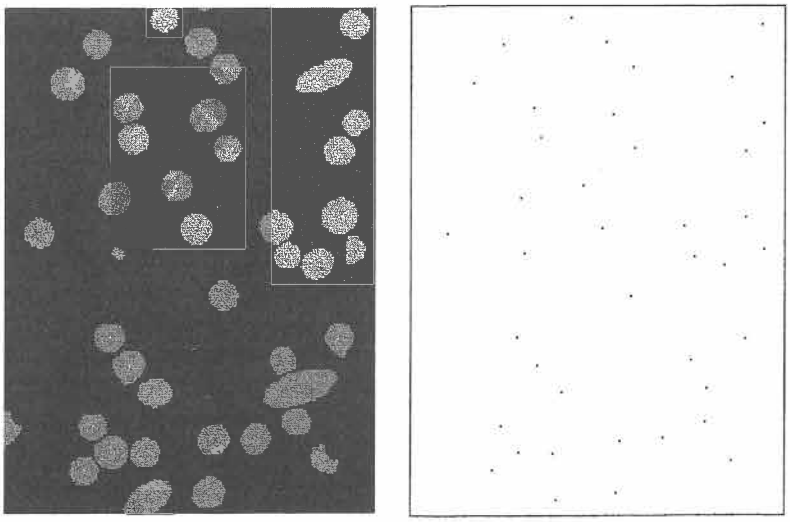

Treated binary image (detail)

Position of the different centroids (white points)

Image formed by the different centroids.

Observed punctual process.

Fig. 8. Binary image treatments for the punctual process method.

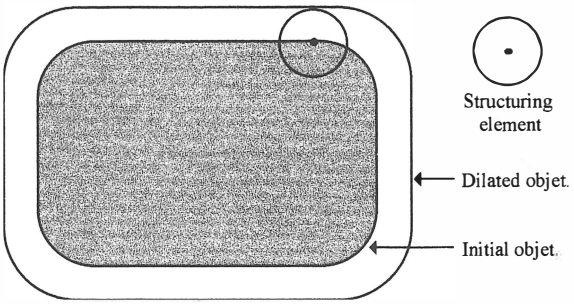

Fig. 9. Presentation of the dilation operation.

of discoid structuring elements of growing diameters in the interparticle area (surface free of fillers) was tested. More precisely, to determine the interparticle distance to the closest neighbour, an original method based on a standard morphological operation (dilation) was developed (see Fig. 9). The grey-level image was filtered and binarised. On the binary image, the different particles were dilated by a hexagonal structuring element. The hexagon is the closest shape to a discoid among the different frameworks. Dilation causes the particles to get bigger and then meet other dilated particles. The number of isolated particles thus decreases. By dilation of increasing size, for each cycle the number of virgin particles that disappear was recorded. A virgin particle was defined as an isolated and dilated particle which had not met another dilated particle during the previous stage of dilation. We can then deduce the distribution of the vanishing individual particles as a function of the size of the hexagonal structuring element (see Fig. 10). The average interparticle distance to the nearest neighbour, d_{1b}, was thus calculated.

The principal bias of this method is a consequence of the use of a hexagonal structuring element on a

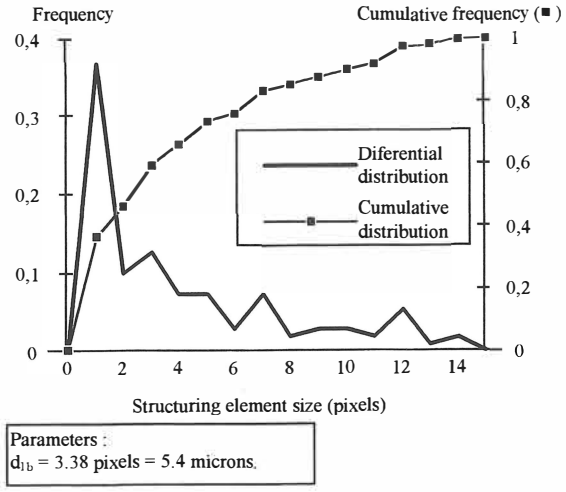

Fig. 10. Presentation of the interparticle distance distribution corresponding to the treatment of the image presented in Figs 5 and 6.

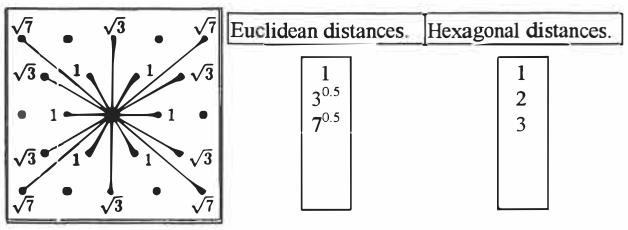

Fig. 11. Illustration of the difference between Euclidean and hexagonal distances.

hexagonal framework. The measurements obtained are not Euclidean distances but hexagonal distances (see Fig. 11).

6 RESULTS

6.1 Intrinsic parameters of the filler: granulometric results

Table 1 shows the main granulometric results. From CFg to SFg2 we can notice a reduction in fibre size owing to the fragmentation process associated with extrusion and injection processing.

Figure 12 shows the granulometric distribution in number for SFg1 and SFg2. It can be seen that it is important to have a global overview of the distribution. In fact, although both number-average lengths are quite close, the size dispersion shapes are different.

Table 1. Size results—average lengths

	L_n (μm)	L_w (μm)
CFg	470	700
SFg1	110	210
SFg2	60	100

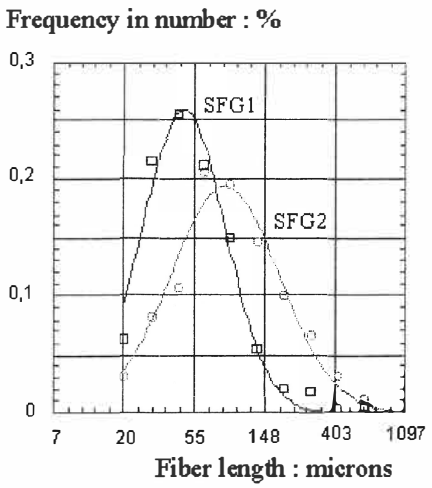

Fig. 12. Fibre length distributions, SFg1 and SFg2 materials.

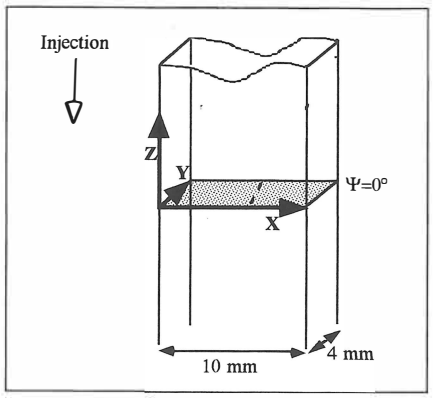

Fig. 13. Representation of section plane.

6.2 Spatial organisation parameters of the filler inside the matrix: orientation and dispersion results

6.2.1 Sampling mode

Most sampling modes for investigations on injected composites take both core and skin behaviour into account.[26,27] However, in some cases it is not possible to discriminate between the two types of layer by microscopic observation. In application of stereological laws, the studied section was shared into zones of equal area. After verification[1] of the existence of two principal symmetry axes in the plane formed by the section through the central part of the injected dumb-bell (see Fig. 13), investigation was limited to a quarter of the section. This was described by 10 different sampling zones: four central and six border zones (see Fig. 14).

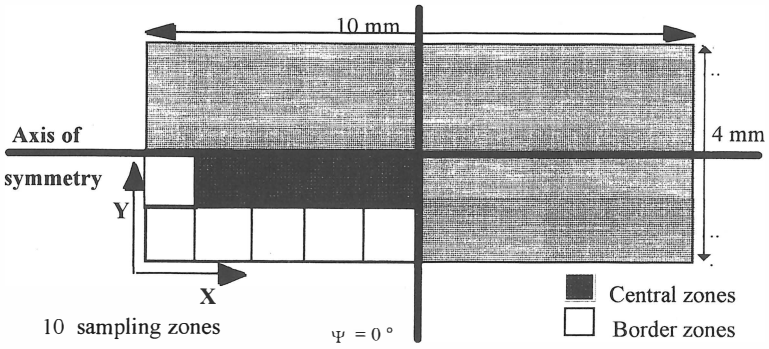

Fig. 14. Sampling zones and symmetry axes.

a_{11} (axis X)		a_{22} (axis Y)		a_{33} (axis Z)	
0.20	0.08	0.03	0.08	0.77	0.85
0.19	0.09	0.01	0.07	0.80	0.84
0.16	0.08	0.01	0.02	0.83	0.89
0.17	0.30	0.00	0.03	0.83	0.68
0.33	0.33	0.00	0.01	0.67	0.65

CFg results.

0.05	0.03	0.07	0.10	0.89	0.87
0.07	0.12	0.03	0.12	0.90	0.76
0.11	0.25	0.02	0.06	0.88	0.69
0.09	0.27	0.02	0.05	0.89	0.67
0.15	0.30	0.03	0.04	0.82	0.66

SFg1 results.

0.19	0.16	0.04	0.08	0.78	0.76
0.13	0.09	0.03	0.21	0.84	0.70
0.16	0.40	0.06	0.11	0.78	0.50
0.35	0.57	0.03	0.05	0.61	0.39
0.44	0.59	0.01	0.02	0.54	0.38

SFg2 results.

Fig. 15. Presentation of the different tensor component data for each sampled zone (in each case, the bottom right-hand corner is in the centre of the section plane).

Each sampling zone was described by four images (microscopic magnification: 400×) to study orientation. But, for the study of dispersion, one image at a lower microscopic magnification (300×) was sufficient.

6.2.2 Orientation results

The results of the three components of the second-order tensor, a_{11}, a_{22} and a_{33}, are presented in Fig. 15. We can notice that, for border zones, fibres are principally parallel to the flow direction (skin behaviour). Fibres tend to be parallel to the principal mould wall. For more central zones, fibres tend to be more transverse to the direction of injection (core behaviour). From CFg to SFg2, shorter fibres tend to be more perpendicular to the injection flow, which is in agreement with the known fibre behaviour inside the flow as a function of the particle size,[26] smaller particles being more mobile.

6.2.3 Dispersion results

6.2.3.1 *Area fractions* Table 2 shows a comparison between the volume fraction results and the average area fraction results. The volume fraction was calculated from the experimental weight fraction. These latter results were obtained by pyrolysis and weighing operations. We can note that the different weight fractions are close to the theoretical 30 wt%. The area fraction averages and the volume fractions seem to be in agreement with stereological laws.[5] In fact, in some particular conditions, stereological laws allow results in a two-dimensional space to be extrapolated to three dimensions. Thus we can assess an equality between area fraction and volume fraction.

By observing detailed results (see Table 3) a slight difference can be shown between the border and centre of the sample. A greater fraction can be noted in the centre of the specimen. These results seem to be in good agreement with those of Spahr *et al.*[28]

6.2.3.2 *Punctual processes* The different R and Q results are presented in Table 4. We can note that the punctual systems studied show similar characteristics to a hard-core stochastic process. In fact, for each point we have an exclusion zone corresponding at least to the fibre diameter. The different data show that the punctual processes obtained for each product are described by almost the same parameters. The shortest intercentre distance, d_{1c}, which is deduced from the density of the observed punctual process, cannot discriminate between the different materials tested (see Table 4). d_{1c} depends more on the area fraction or on the volume fraction, which is almost constant in our case, than on the filler length.

Table 2. Weight fraction, volume and area fraction results

	CFg	SFg1	SFg2
Weight fraction	0·294	0·304	0·307
Volume fraction	0·126	0·131	0·133
Average area fraction	0·119	0·127	0·127
(Standard deviation)	(0·013)	(0·016)	(0·022)

Table 3. Area fraction results detailed for border and centre zones

	Average area fraction	
	Border zones	Centre zones
CFg	0·1170	0·1213
SFg1	0·1268	0·1273
SFg2	0·1270	0·1272

Table 4. Punctual process, interparticle distance and particle radius results

	CFg	SFg1	SFg2
Q factor (d_{1c} ratio)	1·22	1·20	1·19
R factor (standard deviation s^2_{1c} ratio)	0·81	0·89	0·79
Average intercentre distance, d_{1c} (μm)	21·1	21·2	21·2
Average interparticle distance, d_{1b} (μm)	6·6	6·4	5·4
Average particle radius (μm)	14·5	14·8	15·8

6.2.3.3 *Closest interparticle distances (border to border),* d_{Ib} The different d_{1b} values for each product tested are presented in Table 4. We can note that the interparticle distances increase when the fibre length increases. The longer the fibres are, the more they turn parallel to the injection direction and the smaller the elliptical mark. This trend is confirmed by other results relating to centre and border zones. For a given average fibre length, the parameter d_{1b} depends on the orientation situation (skin and core behaviour).

6.2.3.4 *Determination of the average particle radius* In order to verify the different distance results and also to validate the method, an estimation of the average particle radius can be obtained from the difference between d_{1c} and d_{1b}. In Table 4, it can be noted that the average particle radius is close to the fibre diameter: 14 μm. Together with the reproducibility of the tests performed, these results validate the different methods used to quantify the dispersion. The average particle radius depends on the values of d_{1b} (d_{1c} is quasi constant). It increases when the fibre length decreases, from SFg2 to CFg. The orientation results show that the shorter the fibres, the more they tend to run transversally to the flow and the greater the elliptical mark on the surface perpendicular to the injection direction. The projected particle radius therefore depends on the initial fibre length, which induces a typical orientation tendency.

7 DISCUSSION

In addition to reproducibility, which was tested for each method developed, the principal microtextural results

(granulometry, 3D orientation and dispersion) obtained agree with the literature on reinforced thermoplastics. These agreements could appear as a validation of the different techniques.

According to our knowledge, no studies on 3D dispersion determination have been performed with rod fillers. Some models have been proposed,[29] but they are only preliminary approaches. The next step must be the development of techniques for determinations of 3D dispersion by using appropriate spatial models. We have proposed in some papers[1,10,30] relationships between some mechanical properties and some microtextural parameters, but we intend to generalise these approaches on all the determined microtextural parameters. This could be done through the development of appropriate mechanical models.

8 CONCLUSIONS

This paper shows the great interest of techniques based on image analysis, in the determination of material characteristics such as different microtextural parameters. Different automatic or semi-automatic tools were developed, by using optical techniques (granulometry) and scanning electronic microscopy (orientation and dispersion).

The various injected materials studied were different with respect to their average fibre length distribution. The filler ratio and the processing conditions were kept constant. The fibre length of the material inside the matrix was measured. The effect of these filler-size variations on the development of orientation and on dispersion was investigated.

Our general approach and the different methods developed were focused on a selected type of filler (short glass fibres) but they could be applied to treat other kinds of filler and matrix with a few adaptations.

The granulometric techniques which we have developed enabled us to determine fibre length and also to have a feedback control on the processing. The three-dimensional orientation results show the different behaviour inside the sample (skin and core zones) and their relationship with the fibre lengths.

In this paper, we have placed much emphasis on different techniques for measuring dispersion. From the different results we noticed that the dispersion is correlated with other microtextural parameters. By selecting an appropriate descriptor, such as the interparticle distance, d_{1b}, we notice that, for the same filler ratio, variations in the average fibre length cause variations in the dispersion.

REFERENCES

1. Avérous, L., Etude par analyse d'images de la microtexture d'un polypropylène chargé fibres de verre broyées. Relation avec les propriétés du matériau. Ph.D. Thesis, Ecole Nationale Supérieure des Mines de Paris, 1995.
2. Krenchel, H., *Fibre Reinforcement*. Akademisk Folag, Copenhagen, 1964.
3. Cox, H. L., The elasticity and strength of paper and other fibrous materials. *Br. J. Appl. Phys.*, 1952, **3**, 72–79.
4. Guild, F. J. and Summerscales, J., Microstructural image analysis applied to fibre composite materials: a review. *Composites*, 1993, **24**, 383–393.
5. Coster, M. and Chermant, J. L., *Précis d'analyse d'images*. Presses du CNRS, Paris, 1989.
6. Serra, J., *Image Analysis and Mathematical Morphology*, Vol. 1. Academic Press, London, 1982.
7. Lunt, J. M. and Shortall, J. B., The effect of extrusion compounding on fibre degradation and strength properties in short glass-fibre-reinforced nylon 6·6. *Plast. Rubber Process. Applic.*, 1979, **4**, 108–114.
8. Carling, M. J. and Williams, J. G., Fiber length distribution effects on the fracture of short-fibre composites. *Polym. Compos.*, 1990, **11**, 307–313.
9. Ulrych, F., Sova, M., Vokrouhlecky, J. and Turcic, B., Empirical relations of the mechanical properties of polyamide 6 reinforced with short glass fibers. *Polym. Compos.*, 1993, **14**, 229–237.
10. Avérous, L., Quantin, J. C., Lafon, D. and Crespy, A., Granulometric characterization of short fiberglass in reinforced polypropylene. Relation to processing conditions and mechanical properties. *Int. J. Polym. Anal. Characterisation*, 1995, **1**, 339–347.
11. Fischer, G. and Eyerer, P., Measuring spatial orientation of short fiber reinforced thermoplastics by image analysis. *Polym. Compos.*, 1988, **9**, 297–304.
12. Toll, S. and Andersson, P. O., Microstructural characterization of injection moulded composites using image analysis. *Composites*, 1991, **22**, 298–306.
13. Clarke, A. R., Davidson, N. and Archenhold, G., Measurements of fibre direction in reinforced polymer composites. *J. Microsc.*, 1993, **171**, 69–79.
14. Avérous, L., Quantin, J. C., Lafon, D. and Crespy, A., Determination of 3D fibre orientations in reinforced thermoplastics, using scanning electron microscopy. *Acta Stereologica*, 1995, **14**, 69–74.
15. Avérous, L., Quantin, J. C., Lafon, D. and Crespy, A., Evolution of the three-dimensional orientation of glass fibers in injected isotactic polypropylene. *Polym. Eng. Sci.*, 1997, **37**, 329–337.
16. Ess, J. W., Hornsby, P. R., Lin, S. Y. and Bevis, M. J., Characterisation of dispersion in mineral filled thermoplastics compounds. *Plast. Rub. Process. Applic.*, 1984, **4**, 7–14.
17. Chermant, J. L. and Coster, M., Granulometry and granulomorphy by image analysis. *Acta Stereologica*, 1991, **10**, 7–23.
18. Advani, S. G. and Tucker III, C. L., A tensor description of fibre orientation in short fibre composites. *ANTEC'85*, 1985, pp. 1113–1118.
19. Advani, S. G. and Tucker, C. L., III, The use of tensors to describe and predict fibre orientation in short fibre composites. *J. Rheol.*, 1987, **31**, 751–784.
20. Schwarz, H. and Exner, H. E., The characterisation of the arrangement of feature centroids in planes and volumes. *J. Microsc.*, 1983, **129**, 155–169.
21. Shehata, M. T., in *Application of Image Analysis in Characterising Dispersion of Particles*, ed. W. Petrucks. Mineralogical Association of Canada, Ottawa, 1989, Ch. 14, pp. 119–132.
22. Ripley, B. D., Modeling spatial patterns. *J. Roy. Statist. Soc.*, 1977, **B39**, 172–192.

23. Ripley, B. D., *Spatial Statistics*. John Wiley and Sons, New York, 1981.
24. Stoyan, D., Kendall, W. S. and Mecke, J., *Stochastic Geometry and its Applications*. John Wiley and Sons Ltd, Chichester, 1987.
25. Saxl, I., Pelikan, K., Rataj, J. and Besterci, M., *Quantification and Modelling of Heterogeneous Systems*. Cambridge International Science Publishing, Cambridge, 1995.
26. Bailey, R. and Rzepka, B., Fibre orientation mechanisms for injection molding of long fibre composites. *Int. Polym. Process.*, 1991, **VI**, 35–41.
27. O'Connell, A. and Duckett, R. A., Measurements of fibre orientation in short-fibre-reinforced thermoplastics. *Compos. Sci. Technol.*, 1991, **42**, 329–347.
28. Spahr, D. E., Friedrich, K., Schultz, J. M. and Bailey, R. S., Microstructure and fracture behaviour of short and long fibre-reinforced polypropylene composites. *J. Mater. Sci.*, 1990, **25**, 4427–4439.
29. Pelikan, K., Saxl, I. and Ponizil, P., Germ-grain model of short-fibre composites. In *Proceedings of STERMAT 94*, Beskidy Mountains, Poland, 1994, pp. 389–396.
30. Avérous, L., Quantin, J. C., Lafon, D. and Crespy, A., Estimated approach in the determination of elastic modulus for composites with thermoplastic matrix. In *Proceedings of JNC-10*, Vol. 2. AMAC, Paris, 1996, pp. 875–881.